ST open

RESEARCH ARTICLE

Statistical comparison of particle- and detector-level photon distributions obtained with different PYTHIA tunes

Marko Husar, Nikola Poljak

Department of Physics, University of Zagreb Faculty of Science, Zagreb, Croatia

Aim: To investigate how the choice of tuning in the PYTHIA Monte Carlo simulator influences the properties of final-state particles produced in proton–proton collisions, with particular emphasis on regions of phase space that are not typically constrained during the tuning procedure.

Methods: A total of 6×10^8 proton-proton collisions were generated at center-of-mass energies between 100 GeV and 13.6 TeV. PYTHIA Tunes 05, 14, and 21 were investigated. The resulting event samples were compared using a range of statistical tests applied to particle kinematic distributions. Furthermore, an independent simulation of particle energy deposition in detector components corresponding to real experiments is performed, enabling comparisons of energy distributions in both central and forward detectors.

Results: Significant statistical differences were observed between the distributions obtained with different tunes, both for particle kinematics and for energy deposition in the central and forward detector regions. The analysis identifies the tunings that exhibit the largest deviations from one another. Local deviations of up to 44% in the forward detector energy deposition were observed.

Conclusions: The study demonstrates that tuning choices can lead to measurable differences even outside the regions for which they were optimized. It also estimates the amount of data a real central detector would need to collect to experimentally distinguish between simulated distributions produced by different PYTHIA tunings.

Keywords: PYTHIA; generator tuning; Monte Carlo event generators; detector simulation; particle distributions

Correspondence to:
Marko Husar
University of Zagreb, Faculty of Science
Bijenička cesta 32, 10000 Zagreb, Croatia
mhusar.phy@pmf.hr, *marko.husar@cern.ch*

Cite as:
Husar M, Poljak N. Statistical Comparison of Particle- and Detector-Level Photon Distributions Obtained with Different PYTHIA Tunes. ST-OPEN. 2026;7: e2026.2502.5

DOI:
https://doi.org/10.48188/so.7.11

Introduction

In high-energy physics (HEP), Monte Carlo event generators are widely used to model particle collisions. Distributions obtained from such simulations play a crucial role in testing the agreement between theory and experiment, in planning future measurements, and in validating both the generators and detector performance.

Event generators rely on quantum chromodynamics (QCD) together with phenomenological and stochastic models to describe particle production. At leading order, the running of the strong coupling constant α_s is given by Thomson (*1*).

$$1) \qquad \alpha_s(q^2) = \frac{\alpha_s(q_0^2)}{1 - \frac{\beta_0}{4\pi}\alpha_s(q_0^2)\, ln\,(\frac{q^2}{q_0^2})}$$

Here, $\beta_0 = 2/3N_f - 11/3N_c$. In the standard model ($N_f = 6$, $N_c = 3$), $\beta_0 < 0$, implying a decrease of α_S with increasing momentum transfer, in agreement with experimental measurements (*2*, *3*). While perturbative calculations are applicable at large momentum scales, non-perturbative effects dominate at low scales, motivating the use of phenomenological tuning of Monte Carlo generators.

In this paper, the impact of tuning choices is investigated using transverse momentum (p_T) distributions of photons produced in proton-proton (pp) collisions. The transverse momentum is defined as

$$2) \qquad p_T = \sqrt{p_x^2 + p_y^2}$$

in a right-handed coordinate system where the z-axis is aligned with the direction of the colliding proton beams. The transverse plane is defined as the plane perpendicular to this axis, reflecting the approximate cylindrical symmetry of collider detectors.

Existing generator tunes are primarily constrained by measurements in the central detector region and are known to provide a good description of central observables. However, their predictive power in the forward region remains less well constrained. This work, therefore, examines how tuning choices optimized for central region affect particle-level and detector-level observables in both the central and forward regions, with particular emphasis on whether different PYTHIA tunes can be experimentally distinguished at the detector level.

We chose photons as probes for these comparisons, since they are mostly unscathed by interactions in the central parts of the detector and are often used in real-world forward measurements. Furthermore, photon energy loss can be modelled in a simple and robust way, which makes them an ideal candidate for detector simulations.

Methods

Simulation and tuning setup

PYTHIA is a general-purpose Monte-Carlo event generator for the simulation of high-energy particle collisions, incorporating models for a wide range of physical processes, including hard and soft QCD interactions, parton distribution functions, parton showering, hadronization, and particle decays (*4*). It is one of the most widely used event generators in particle physics. In this work, PYTHIA, version 8.312, is used to simulate high-energy *pp* collisions, with both soft and hard QCD processes enabled. A fixed random seed (0) is used to ensure reproducibility.

Many processes in hadronic collisions, including hadronization and multiparton interactions, are governed by non-perturbative QCD dynamics and cannot be calculated from first principles. While the corresponding model parameters in PYTHIA may formally be adjusted independently, physical constraints introduce non-trivial correlations among them. As a result, these parameters are optimized through global tuning procedures, yielding coherent parameter sets, commonly referred to as *tunes*, which are designed to reproduce experimental findings.

In this study, three different PYTHIA tunes are compared:

- Tune 14 (Monash 2013) (*5*), which serves as a standard reference tune for *pp* collisions and provides a good description of measurements in central Large Hadron Collider (LHC) detectors;
- Tune 05(4C) (*6*) developed to reproduce early LHC data and featuring a reduced diffractive cross section, which played an important role in the early validation of PYTHIA for LHC analyses (*7*);
- Tune 21 (Atlas A14) (*8*), optimized using measurements from the central region of ATLAS experiment.

Event generators

In particle physics, the outcome of a single collision or decay process is referred to as an event. Due to the intrinsic probabilistic nature of quantum processes, the number and properties of final-state particles vary from event to event. Event generators are numerical tools designed to produce ensembles of such simulated events, with the aim of predicting experimentally accessible observables. In the case of PYTHIA 8, these predictions depend on of order one hundred model parameters (*4*) whose values are determined through comparisons with experimental data and collectively define a given tune.

Statistical analysis

Normalized histograms and statistical uncertainties

Distributions are visualized using histograms, where the variable range is divided into 50 equidistant bins covering the interval between the minimum and maximum measured values, with bin contents representing the corresponding frequencies. Since different data samples are compared, all histograms are normalized such that the sum of relative bin frequencies equals unity, removing any dependence on the total number of events.

The relative frequency in the i-th bin is defined as $f_{r,i}=f_i/N$, where f_i is the number of entries in the bin and N is the total number of events distributed over ξ bins. Assuming Poisson statistics, the absolute uncertainty of each bin, σ_i, is given by the square root of the number of entries in the bin.

The uncertainty of the normalized bin content is obtained using standard error propagation for correlated variables, yielding

$$3) \qquad \sigma_{r,i}=\sqrt{\left(\frac{N-f_i}{N^2}\right)^2\frac{1}{f_i}+\left(\frac{f_i}{N^2}\right)^2\sum_{j=i}\frac{1}{f_i}}$$

This expression accounts for correlations introduced by the normalization constraint, whereby the uncertainty of each bin depends on the statistical uncertainties of all bins.

Statistical tests for distribution comparison

To quantify differences between distributions obtained with different generator tunes, three statistical tests are employed: the Kolmogorov–Smirnov test, the analysis of variance (ANOVA), and the Kruskal–Wallis test. For each test, the null hypothesis assumes that the compared distributions are drawn from the same parent distribution. The statistical significance of the results is assessed using the corresponding p-values, with distributions considered significantly different for $P \leq 0.05$.

All three tests are implemented in SciPy, version 1.14.1, and are accessed through its standard statistical analysis routines.

Kolmogorov–Smirnov test

The Kolmogorov–Smirnov test is a non-parametric method for comparing one-dimensional probability distributions (*9*, *10*). In this work, the two-sample version of the test is used to compare distributions generated with different tunes. The Kolmogorov–Smirnov statistic is defined as

$$4) \qquad D_{\alpha,\beta}=\sup_x|X_\alpha(x)-X_\beta(x)|$$

where X_α and X_β are the empirical cumulative distribution functions of two samples. The Kolmogorov–Smirnov statistic quantifies the maximum difference between the cumulative distributions and is therefore sensitive to differences in distribution shape.

ANOVA test

ANOVA is a parametric method based on *F*-tests that compares the means of two or more samples by analysing their variances (*11*). The null hypothesis is rejected when the resulting *F*-statistic exceeds the corresponding critical value. For normalized histograms with ξ bins, the number of degrees of freedom is $DoF = \xi - 2$, accounting for the normalization constraint and the fixed total event count. The ANOVA test assumes that data from different bins are not correlated, and its results are valid only under this assumption. Since ANOVA assumes normally distributed samples, its applicability may be limited for distributions that deviate significantly from Gaussian behaviour.

Kruskal–Wallis test

The Kruskal–Wallis test is a non-parametric alternative to ANOVA that does not assume normality of the underlying distributions (*12*). The Kruskal–Wallis test assesses whether two samples are drawn from the same underlying distribution by quantifying the maximum absolute deviation between their cumulative distribution functions. The Kruskal–Wallis statistic thus probes the largest global difference between cumulative distribution functions, rather than local bin-to-bin fluctuations. This test is particularly well suited for asymmetric distributions or distributions with long tails, where the assumptions of ANOVA are not fulfilled. The null hypothesis is rejected when the corresponding *H*-statistic exceeds the critical value.

Results

Transverse momentum distributions of photons produced in *pp* collisions are studied in the center-of-mass frame, $E_{CM}{}^2 = s$, at $E_{CM} = 100$ GeV, independent of the identity of the parent particle. In addition, photon distributions originating from the decay of neutral pions

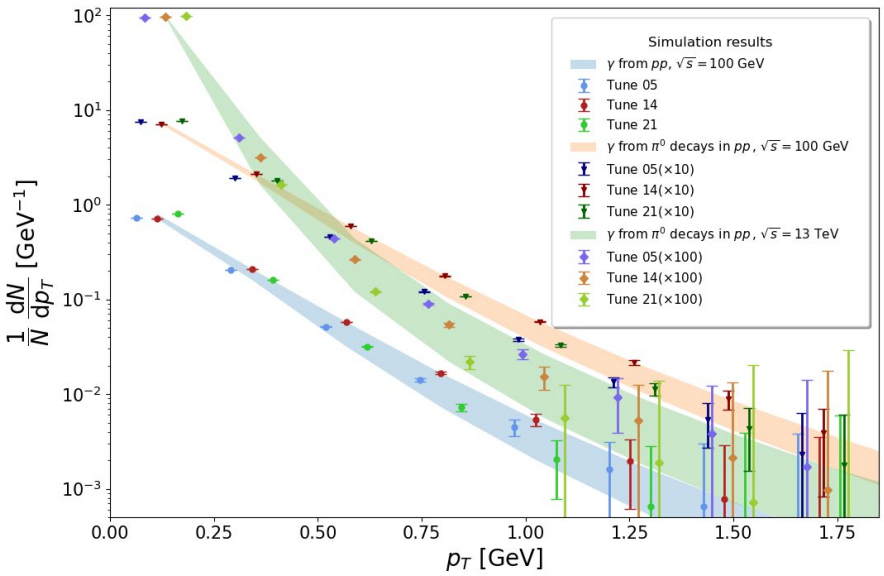

Figure 1. Simulated photon transverse momentum distributions for three different production scenarios, shown for three PYTHIA 8 tunes in each case. Distributions of photons originating from pion decays at 100 GeV (13 TeV) are multiplied by a factor of 10 (100), respectively, to enhance visibility.

are analysed for *pp* collisions at E_{CM} = 100 GeV and E_{CM} = 13 TeV. Neutral pions are chosen as parent particles due to their abundant production in the region close to the beam axis in hadronic collisions (*13*). The π^0 meson has a mean lifetime of $\tau(\pi^0) = (8.43 \pm 0.13) \times 10^{-17}$ s and decays predominantly into two photons, with a branching ratio of $BR(\pi^0 \rightarrow 2\gamma) = (98.8$ $23 \pm 0.034)\%$ (*14*).

For each of three scenarios, 1.5×10^7 *pp* collisions were simulated for each tune. Normalized histograms of the resulting photon transverse momentum distributions are shown in **Figure 1**, with different shaded regions indicating the three production scenarios. The distributions are presented only up to a certain value of p_T, corresponding to the region where differences between tunes are expected to be most pronounced. At higher transverse momenta, the relative differences between distributions are consistent with statistical uncertainties, indicating no significant deviations within the simulated data sample. The error bars shown in **Figure 1** represent the standard deviations of the relative bin frequencies, as defined in equation 3.

To quantify the differences between tunes, the relative differences between the *i*-th bin of distributions generated with tunes *a* and *b* is defined as

$$\Delta_{r,i}^{a,b} = \frac{|f_{r,i}^a - f_{r,i}^b|}{\sqrt{(f_{r,i}^a + f_{r,i}^b)/2}} \qquad 5)$$

The relative difference between two quantities is conventionally defined as the ratio of their difference to their average. In the definition of Δ_r, the square root in the denominator is introduced in order to express the difference between relative frequencies in units of their statistical uncertainty. This formulation is applicable as long as the compared quantities are dimensionless, as is the case for normalized histogram bin contents. Equation 5 therefore defines a discrete quantity evaluated independently for each histogram bin. We emphasize that the relative difference defined in equation 5 is not equivalent to the Kolmogorov–Smirnov statistic $D_{a,b}$ or to any of other discussed statistical measures used to compare distributions generated with tunes *a* and *b*.

Statistical analysis of photon p_T spectra in pp collisions at E_{CM} = 100 GeV

In **Figure 2**, Panel A shows the relative differences between data sets obtained from simulations using different PYTHIA tunes. From equation 5, this quantity is a discrete variable. The lines connecting the points in **Figure 2** are included solely to guide the eye. The largest relative differences are observed between the distributions with tunes 14 and 21. As expected, the differences are most pronounced in low-p_T region, while no significant deviations are observed at high transverse momenta. Since particles with large p_T are predominantly produced in the central detector region, where all tunes are constrained by experimental measurements, the observed differences in this region are small. Residual discrepancies arise from differences in tuning choices but remain small for the simulated data sample.

To quantitatively assess the agreement between the distributions, the statistical tests described before are applied. The results of the Kolmogorov–Smirnov, ANOVA, and Kruskal–

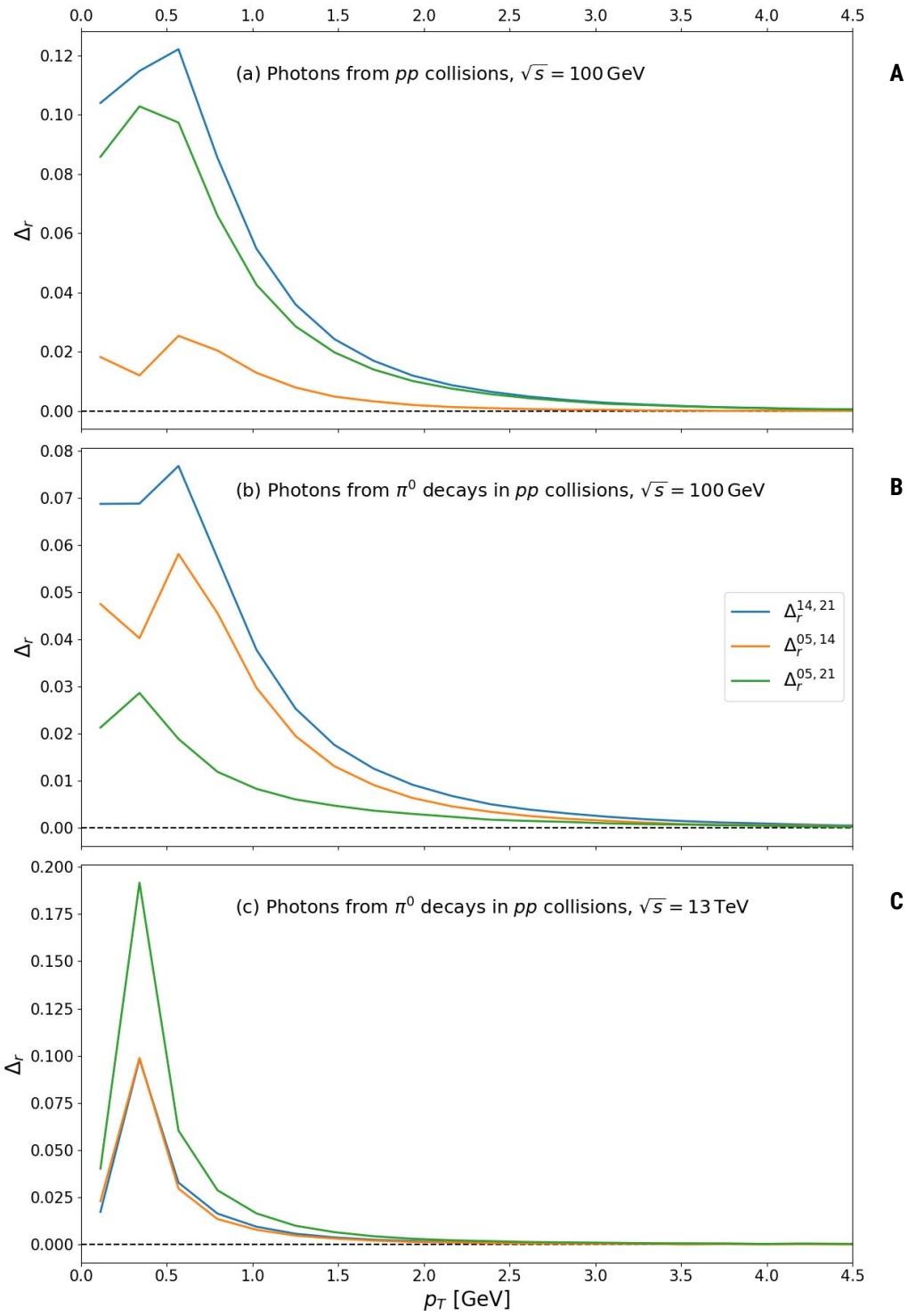

Figure 2. Panel A. Relative differences between photon p_T spectra in pp collisions at $E_{CM} = 100$ GeV for different generator tunes. **Panel B.** Relative differences between photon p_T spectra from π^0 decays in pp collisions at $E_{CM} = 100$ GeV for different generator tunes. **Panel C.** Relative differences between photon p_T spectra from π^0 decays in pp collisions at $E_{CM} = 13$ TeV for different generator tunes.

Wallis tests are summarized in **Table 1**. For example, a value of $D_{05,14} = 0.075$ indicates that the maximum difference between the cumulative distributions corresponding to tunes 05 and 14 is 7.5%, while $D_{05,21} = 0.175$ corresponds to a maximum difference of 17.5% between the tunes 05 and 21. Since all obtained P-values are well above the threshold of 0.05, no global incompatibility is found at $\alpha = 0.05$ when the full spectrum is considered.

Table 1. Results of statistical tests for photon transverse momentum distributions in *pp* collisions at E_{CM} = 100 GeV

Tunes	05, 14	05, 21	14, 21
D	0.0750	0.1750	0.1500
p^D	0.9999	0.5786	0.7659
F	0.0003	0.0133	0.0101
p^F	0.9866	0.9085	0.9203
H	0.0628	1.0026	1.6501
p^H	0.8021	0.3167	0.1989

The statistical tests consistently indicate that the transverse momentum distributions of photons generated with different tunes are compatible within statistical uncertainties when considering the full p_T range. This result is expected, as the region where the distributions differ most – the low-p_T-region – constitutes only a small fraction of the overall p_T spectrum. Nevertheless, relative differences of up to 17.5% are observed locally, which is relevant for precision simulations of low-p_T photons. Such simulations are of particular importance for the design and interpretation of experiments in forward detector regions.

Statistical analysis of photon p_T spectra from π^0 decays in pp collisions at E_{CM} = 100 GeV

Photon transverse momentum distributions from neutral pion decays produced in *pp* collisions at E_{CM} = 100 GeV are analysed. The relative differences between the tunes are presented in **Figure 2**, Panel B.

As in the case of inclusive photons, the largest differences are observed in the low-p_T region. In contrast to the previous case, the smallest relative differences are found between tunes 05 and 21, while the largest differences remain between the tunes 14 and 21. The results of the statistical tests applied to these distributions are summarized in the **Table 2**. The KS statistic indicates maximum relative differences of up to 12.5% in the low-p_T region, while all corresponding p-values exceed 0.05, indicating no statistically significant differences when the full p_T range is considered.

Table 2. Results of statistical tests for photon transverse momentum distributions from pion decays in *pp* collisions at E_{CM} = 100 GeV

Tunes	05, 14	05, 21	14, 21
D	0.0750	0.1250	0.1250
p^D	0.9999	0.9188	0.9188
F	0.0002	0.0130	0.0106
p^F	0.9891	0.9094	0.9181
H	0.0783	0.4140	0.7013
p^H	0.7796	0.5199	0.4024

Statistical analysis of photon p_T spectra from π^0 decays in pp collisions at E_{CM} = 13 TeV

Photon transverse momentum distributions from π^0 decays produced in *pp* collisions at E_{CM} = 13 TeV are analysed to probe tune-dependent effects at energies relevant for current LHC operations. The relative differences between distributions obtained with different tunes are shown in **Figure 2**, Panel C. As in the lower-energy case, the largest differences are observed in the low-p_T region, and the distributions are once again shown up to a p_T value where relative differences exceed the corresponding statistical uncertainties.

In contrast to the E_{CM} = 100 GeV case, the largest relative differences at E_{CM} = 13 TeV are observed between the tunes 05 and 21. The Kolmogorov–Smirnov statistic yields a maximum difference of $D_{05,21}$ = 0.1846, corresponding to a relative deviation of 18.46%. Nevertheless, all statistical tests indicate that the distributions remain statistically compatible when the full p_T range is considered, with all *P*-values exceeding the threshold. The results of the statistical tests are summarized in **Table 3**.

Table 3. Results of statistical tests for photon transverse momentum distributions from pion decays in *pp* collisions at E_{CM} = 13 TeV

Tunes	05, 14	05, 21	14, 21
D	0.0923	0.1846	0.1231
p^D	0.9473	0.2190	0.7126
$F/\times10^{-5}$	3.1423	0.0009	3.3468
p^F	0.9955	0.9998	0.9954
H	0.6027	2.6832	0.6339
p^H	0.4376	0.1014	0.4259

A comparison between the lower-energy results demonstrates that tune-dependent differences are sensitive to the collision energy. This indicates that precision simulations of low-p_T photon distributions require a careful assessment of tuning effects at the specific center-of-mass energy of interest.

Detector response and energy deposition

So far, photon transverse momentum distributions have been analysed as intrinsic particle-level quantities obtained directly from PYTHIA. To assess whether the observed tune-dependent differences can be detected experimentally, photon energy distributions are propagated through a detector model, and the corresponding detector response is simulated.

An electromagnetic calorimeter is modelled using a homogeneous scintillating material. Proton-proton collisions are generated, and photons produced in the simulated events are selected, independently of their production mechanism. For each photon, the production vertex and four-momentum are used to reconstruct its trajectory. If a photon intersects the detector volume, its initial energy and total path length traversed inside the detector are recorded and used as input for the detector response simulation.

Photon interactions with matter are dominated by electromagnetic processes. In this analysis, energy deposition is modelled using an effective attenuation approach, in which the photon energy decreases exponentially with the path length traversed in the detector material (*15*). The remaining photon energy after traveling a distance x is given by Viehhauser and Weidberg (*16*).

$$6) \qquad E(x) = E_0 \exp\left(-\frac{7}{9}\frac{x}{x_0}\right)$$

where E_0 is the initial photon energy and X_0 is the radiation length of the material. The total energy deposited in the detector is then

$$7) \qquad E_{dep} = E_0 - E(x_{tot})$$

with x_{tot} denoting the total path length inside the detector volume.

The detector material is chosen to be thallium-doped sodium iodide, *NaI*(*Tl*), a commonly used scintillator in electromagnetic calorimetry (*17*, *18*). Its radiation length is taken to be the one provided by Navas *et al.* (*14*).

$$8) \qquad X_0(NaI) = 2.62\ cm$$

Distributions of photon energy deposited in the central and forward detectors are generated for *pp* collisions at $E_{CM} = 7.9$ TeV and $E_{CM} = 13.6$ TeV, corresponding to different operational energies of the LHC. The energy deposition was simulated within the PYTHIA code itself, without employing a full GEANT detector simulation. Previous results have shown that different generator tunes provide a similar description of particle kinematics in the central detector region, close to the interaction point. Here, we investigate whether a realistic central detector can experimentally resolve differences between the simulated energy deposition distributions, either globally or within specific energy ranges. In addition, we estimate the amount of data required for a central detector to observe such differences. Finally, the deposited energy distributions in the central and forward detectors are compared to assess the sensitivity of different detector regions to tuning-dependent effects.

As previously observed, the largest differences between the distributions occur in the low-energy photon spectra. This raises the question of whether a realistic central or forward detector, calibrated for the detection of low-energy photons, can experimentally resolve differences between distributions obtained with different generator tuning choices. To address this, a reduced spectrum of detected photons is analysed.

Simulation of energy deposition in the central detector

A realistic central detector cannot fully enclose the interaction point, as space must be reserved for the beam pipe and the associated superconducting accelerator infrastructure. To model this geometry, the simulated detector is divided into four regions: a main active detector volume and three inactive (“dark”) regions, as illustrated in **Figure 3**. The inactive regions represent volumes occupied by non-sensitive instrumentation in real experiments.

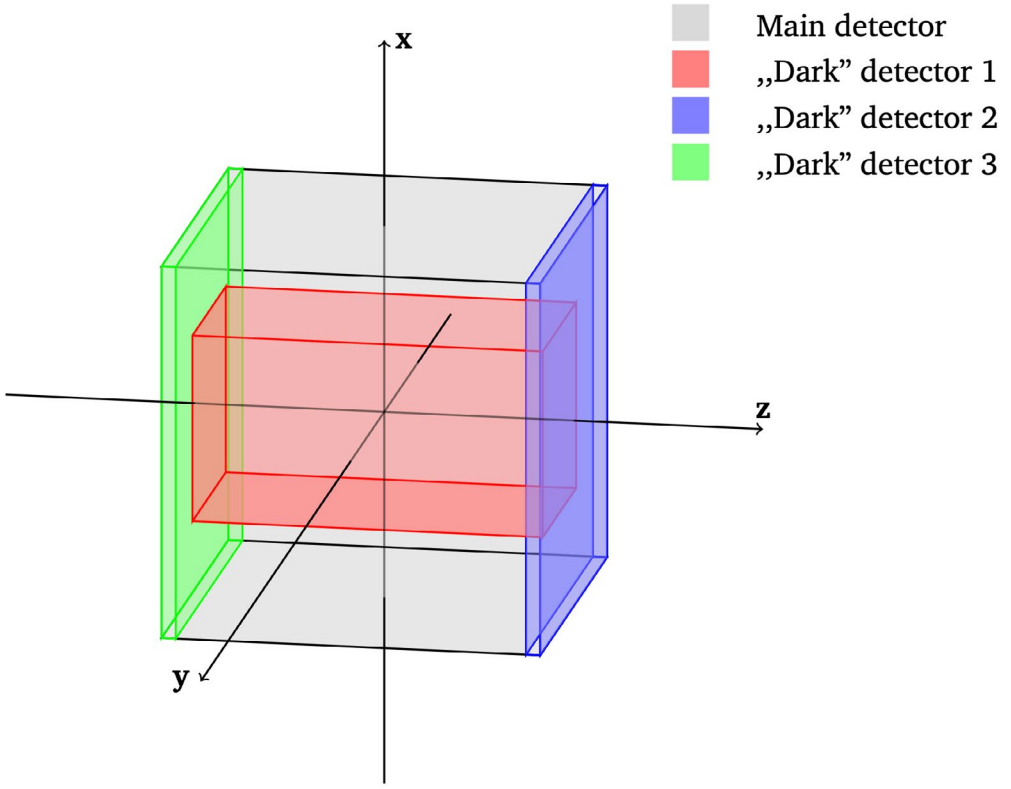

Figure 3. Schematic view of the simulated central detector. The main detector volume is shown in gray, while the inactive ("dark") regions are indicated in red, blue, and green.

The main detector is modelled as a cubic *NaI* volume with dimensions $(80\ \text{cm})^3$. The first inactive region is a rectangular volume of dimensions 40×40×74 cm, centered along the beam (z) axis. Two additional inactive regions, each with dimensions $80 \times 80 \times 3$ cm, are placed adjacent to the main detector along the beam direction.

The deposited energy is calculated using equation 7, which depends only on the total path length through the sensitive detector volume. The effective path length is therefore obtained by subtracting the trajectory segments traversing inactive regions,

$$9) \qquad x_{tot} = x_{main} - \sum_{i=1}^{3} x_{dark}$$

For each tuning configuration, 1.5×10^7 proton-proton collisions are generated at each center-of-mass energy.

Distributions of deposited photon energies in pp collisions at E_{CM} = 7.9 TeV

Figure 4, Panel A shows the normalized histograms of deposited photon energies for three generator tunes. In contrast to previous histogram representations, the first bin corresponding to photon energies $E_\gamma \in (0,0.4]$ GeV is omitted for clarity. The binning is linear, despite the rapid decrease in statistics toward higher-energy bins, rather than logarithmic. Since the analysis focuses exclusively on relative differences and statistical uncertainties are explicitly monitored, there is no methodological requirement to adopt logarithmic bin-

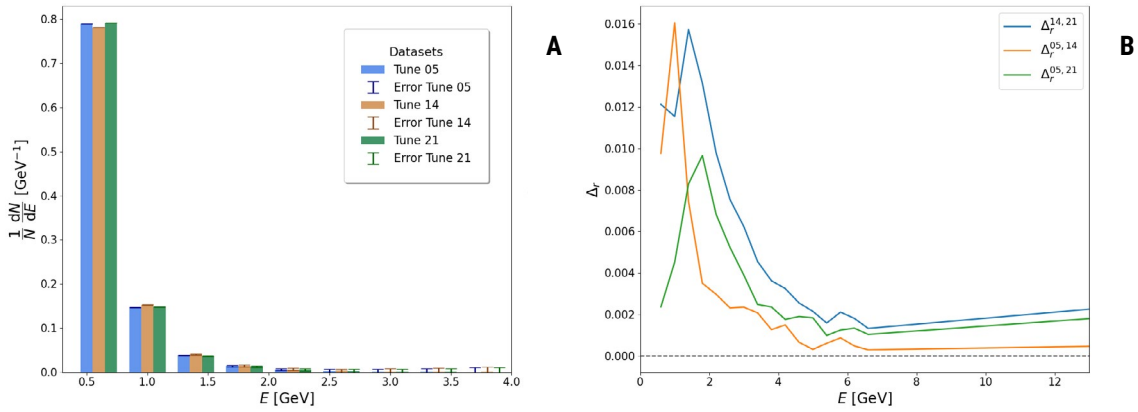

Figure 4. Panel A. Normalized histograms of deposited photon energy distributions in the simulated central detector for *pp* collisions at E_{CM} = 7.9 TeV. **Panel B.** Relative differences between deposited photon energy distributions in the central detector for *pp* collisions at E_{CM} = 7.9 TeV.

Table 4. Results of statistical tests for deposited photon energy distributions in the central detector for *pp* collisions at E_{CM} = 7.9 TeV

Tunes	05, 14	05, 21	14, 21
D	0.1200	0.0800	0.1000
p^D	0.8693	0.9977	0.9667
F	0.0396	0.0043	0.0678
p^F	0.8427	0.9479	0.7949
H	0.1948	0.0457	0.0705
p^H	0.6590	0.8307	0.7906

ning. The linear binning is therefore retained, as only relative deviations between tunes are of interest.

Hadronic collisions produce a large number of low-energy photons, causing the bin to dominate the normalized distribution and obscure higher-energy features. The lowest-energy photons are nevertheless included in all subsequent statistical analyses.

The relative differences between the deposited energy distributions obtained with different tuning choices are computed using equation 5 and are shown in **Figure 4**, Panel B. The observed differences are nearly an order of magnitude smaller than those found at the particle level, consistent with the fact that PYTHIA tunes are optimized to provide a similar description of processes in the central detector region. Statistical tests applied to the distribution shown in **Figure 4**, Panel A, summarized in **Table 4**, confirm that no statistically significant differences are present, with all *P*-values well above 0.05.

A selection on the deposited photon energy is applied by restricting the analysis to $E_{dep} \leq 6$ GeV. Histograms are constructed using the same number of the bins as in the full energy-range analysis in order to allow a direct comparison. The resulting normalized distributions are shown in **Figure 5**, Panel A, with the lowest-energy bin omitted for clarity.

The corresponding relative differences between the distributions obtained with different tuning choices are presented in **Figure 5**, Panel B. Compared to the full-spectrum results,

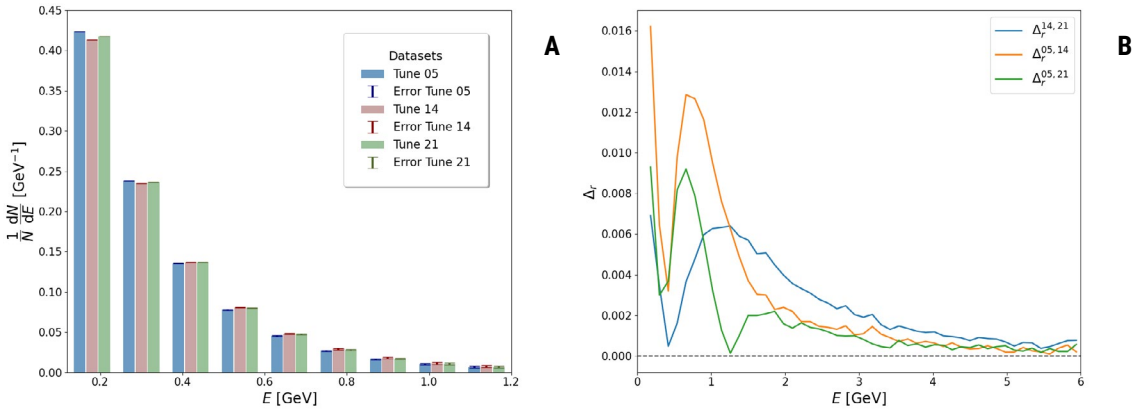

Figure 5. Panel A. Normalized histograms of reduced deposited photon energy distributions in the central detector for *pp* collisions at E_{CM} = 7.9 TeV. **Panel B.** Relative differences between reduced deposited photon energy distributions in the central detector for *pp* collisions at E_{CM} = 7.9 TeV.

Table 5. Results of statistical tests for reduced deposited photon energy distributions in the central detector for *pp* collisions at E_{CM} = 7.9 TeV

Tunes	05, 14	05, 21	14, 21
D	0.0400	0.0400	0.0400
p^D	0.9999	0.9999	0.9999
F	0.0479	0.0052	0.0818
p^F	0.8273	0.9427	0.7754
H	0.0760	0.0023	0.0399
p^H	0.7827	0.9615	0.8415

the relative differences between tunes 14 and 21 are reduced, while larger fluctuations are observed due to the smaller statistical sample induced by energy selection.

The results of the statistical tests, summarized in **Table 5**, indicate that no statistically significant differences are present in the reduced energy range, with all *P*-values exceeding 0.05. This outcome is consistent with the small tune-dependent effects observed in the central detector and confirms the robustness of the generator description in this region.

Distributions of deposited photon energies in pp collisions at E_{CM} = 13.6 TeV

Previous analyses have shown that tune-dependent differences between distributions depend on the center-of-mass energy of the *pp* collisions. To assess whether this energy dependence is observable at the detector level, relative differences between the deposited photon energy distributions at E_{CM} = 7.9 TeV and E_{CM} = 13.6 TeV are compared.

The normalized deposited energy distributions for E_{CM} = 13.6 TeV are shown in **Figure 6**, Panel A. For clarity, the lowest-energy bin is omitted, while visible differences between tunes are observed already in the first displayed bin. The corresponding relative differences, shown in **Figure 6**, Panel B, decrease with increasing deposited energy and approach zero at energies of order 10 GeV. A comparison with the E_{CM} = 7.9 TeV results confirms that the relative differences depend strongly on the collision energy. In particular, while

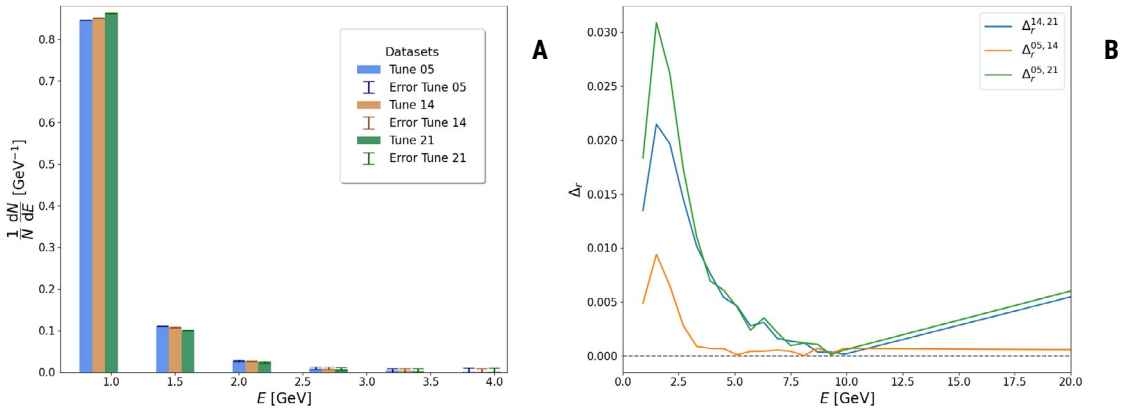

Figure 6. Panel A. Normalized histograms of deposited photon energy distributions in the simulated central detector for *pp* collisions at E_{CM} = 13.6 TeV. **Panel B.** Relative differences between deposited photon energy distributions in the central detector for *pp* collisions at E_{CM} = 13.6 TeV.

Table 6. Results of statistical tests for deposited photon energy distributions in the central detector for *pp* collisions at E_{CM} = 13.6 TeV

Tunes	05, 14	05, 21	14, 21
D	0.1200	0.4000	0.3600
p^D	0.8693	0.0006	0.0028
$F/\times 10^{-3}$	2.7099	2.1236	0.0036
p^F	0.9586	0.9633	0.9952
H	0.2171	4.7040	3.4915
p^H	0.6413	0.0301	0.0617

differences between tunes 05 and 21 were smallest at E_{CM} = 7.9 TeV, they become largest at E_{CM} = 13.6 TeV, demonstrating the sensitivity of tuning effects to the collision energy.

Statistical tests applied to the distributions shown in **Figure 6**, Panel A, summarized in **Table 6**, indicate statistically significant differences. The Kolmogorov–Smirnov test yields the *P*-values below 0.05 for the tune pairs 05–21 and 14–21, indicating significant shape differences, while the Kruskal–Wallis test yields $p_{05,21}{}^H = 0.0301$, pointing to a significant difference in the median. In contrast, the ANOVA test shows no significant differences in the mean value of distributions. These results demonstrate that, despite the similar tuning of generators in the central detector region, measurable differences can be observed at sufficiently high collision energies.

In the present analysis, we used 1.5×10^7 simulated collisions per tune. This number of events was a conservative approximate threshold at which we expect tune differences to become observable. It was inferred from the average number of photons per event and the binning used in the analysis as the number of events required for any tune differences to significantly outweigh the relative lowest bin deviation in a single tune.

Given the effective data-taking rates at the LHC, this corresponds to approximately 10–15 days of continuous data collection for a central detector, providing an estimate of the experimental sensitivity needed to distinguish between different tuning choices.

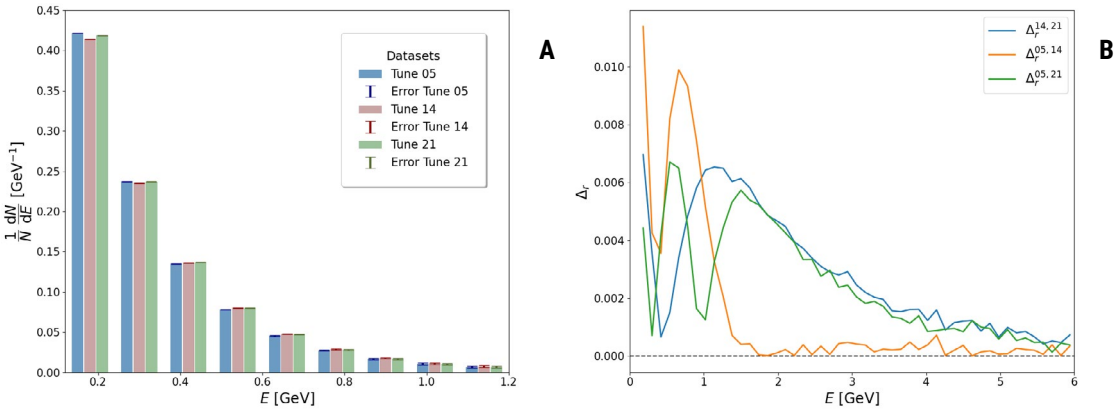

Figure 7. Panel A. Normalized histograms of reduced deposited energy distributions in the central detector for *pp* collisions at E_{CM} = 13.6 TeV. **Panel B.** Relative differences between reduced deposited photon energy distributions in the central detector for *pp* collisions at E_{CM} = 13.6 TeV.

Table 7. Results of statistical tests for reduced deposited photon energy distributions in the central detector for *pp* collisions at E_{CM} = 13.6 TeV

Tunes	05, 14	05, 21	14, 21
D	0.0600	0.0600	0.0800
p^D	0.9999	0.9999	0.0077
$F/\times 10^{-3}$	3.3510	2.6267	0.0044
p^F	0.9540	0.9592	0.9947
H	0.0502	0.0487	0.2070
p^H	0.8227	0.8254	0.6491

As in the previous case, reduced deposited energy distributions in the central detector are examined by applying the same selection, $E_{dep} \leq 6$ GeV. The resulting normalized histograms are shown in **Figure 7**, Panel A. For clarity, the lowest-energy bin corresponding to $E_\gamma \in (0,0.12]$ GeV is omitted, and only bins up to the deposited energy of 1.2 GeV are displayed, as differences at higher energies are comparable to the associated statistical uncertainties.

The corresponding relative differences are presented in **Figure 7**, Panel B. Compared to the full energy spectrum, larger fluctuations are observed, reflecting the reduced statistical sample after the energy selection. While the smallest differences in the full spectrum are found between tunes 05 and 14, the reduced distributions show the largest relative differences for this tune pair. The results of statistical tests, summarized in **Table 7**, indicate that no statistically significant differences are present in the reduced energy range.

This implies that the statistically significant differences observed at E_{CM} = 13.6 TeV in the central detector originate predominantly from higher-energy photons rather than from the low-energy part of the spectrum. Overall, these results demonstrate that tune-dependent differences in deposited energy distributions depend on the collision energy and can be observed in the central detector provided that a sufficiently large data sample is collected.

Simulation of energy deposition in the forward detector

Figure 8 shows a schematic view of the simulated forward detector geometry. As in the central detector case, inactive ("dark") detector regions are introduced to account for the space occupied by the beam pipe. Owing to the detector positioning, only a single inactive region is required in this configuration. The forward detector is located 10 m from the interaction point. The active detector volume is modelled as a *NaI* block with dimensions 80×80×40 cm, while the inactive region is centered along the beam axis and has dimensions 50×50×40 cm. The effective photon path length through the sensitive detector volume is computed using the same method as for the central detector.

For each tuning configuration and collision energy, 4.95×10^7 proton-proton collisions are generated. This larger sample size ensures a comparable number of detected photons with respect to the central detector analysis, allowing a direct comparison of the results. Both the full and reduced deposited energy ranges are examined.

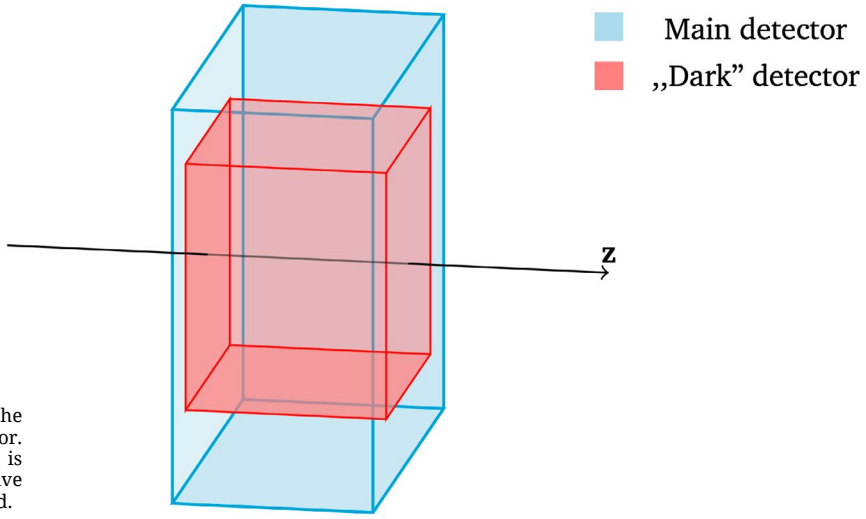

Figure 8. Schematic view of the simulated forward detector. The main detector volume is shown in blue, while the inactive ("dark") region is shown in red.

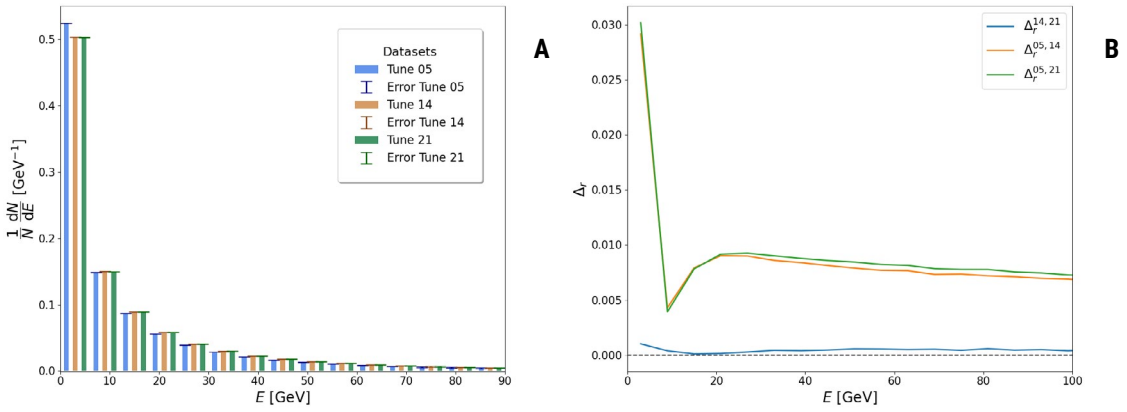

Figure 9. Panel A. Normalized histograms of deposited photon energy distributions in the simulated forward detector for *pp* collisions at E_{CM} = 7.9 TeV. **Panel B.** Relative differences between deposited photon energy distributions in the simulated forward detector for *pp* collisions at E_{CM} = 7.9 TeV.

Distributions of deposited photon energies in pp collisions at E_{CM} = 7.9 TeV

The deposited photon energy distributions for *pp* collisions at E_{CM} = 7.9 TeV are shown in **Figure 9**, Panel A. Qualitatively, differences between tunes are visible primarily in the lowest-energy bin, while at higher energies the relative differences are comparable to statistical uncertainties. The corresponding relative differences, shown in **Figure 9**, Panel B, are small, with $\Delta_{r,i}^{05,14} \approx \Delta_{r,i}^{05,21}$ for all bins, suggesting similar Kolmogorov–Smirnov statistics for these tune pairs.

The results of the statistical tests, summarized in **Table 8**, confirm this observation. All *P*-values exceed the 0.05 significance threshold, indicating no statistically significant differences between the distributions. Consistent with the relative-difference analysis, identical KS statistics are obtained for the tune pairs 05–14 and 05–21.

Since the largest differences are concentrated in the low-energy regions, the analysis is subsequently repeated for reduced deposited energy distributions by applying the same selection as in the central detector study, $E_{dep} \leq 6$ GeV.

The reduced deposited energy distributions in the forward detector are shown in **Figure 10**, Panel A. For visualization purposes, the lowest-energy bin corresponding to photon energies $E_\gamma \in (0, 0.12]$ GeV is omitted, although it is included in the statistical analyses. The

Table 8. Results of statistical tests for deposited photon energy distributions in the forward detector for *pp* collisions at E_{CM} = 7.9 TeV

Tunes	05, 14	05, 21	14, 21
D	0.1000	0.1000	0.0200
p^D	0.9667	0.9667	1.0000
F	0.0175	0.0220	0.0003
p^F	0.8950	0.8823	0.9870
H	0.5240	0.5962	0.0297
p^H	0.4692	0.4401	0.8632

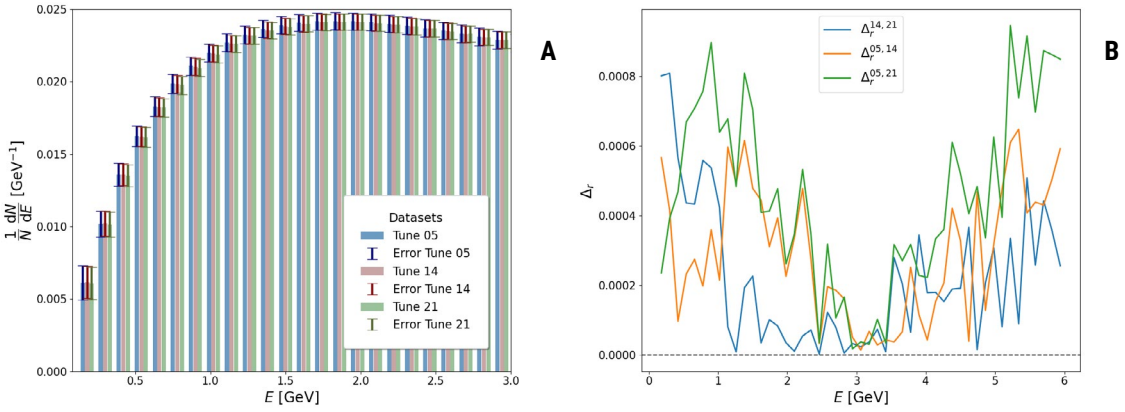

Figure 10. Panel A. Normalized histograms of reduced deposited photon energy distributions in the simulated forward detector for *pp* collisions at E_{CM} = 7.9 TeV. **Panel B.** Relative differences between reduced deposited photon energy distributions in the simulated forward detector for *pp* collisions at E_{CM} = 7.9 TeV.

corresponding relative differences, presented in **Figure 10**, Panel B, exhibit sizable fluctuations that decrease as the deposited energy approaches $E_{dep} \sim 3$ GeV. This behaviour reflects the fact that photons detected in the forward region typically carry higher energies than those observed in the central detector. Consequently, restricting the analysis to $E_{dep} \leq 6$ GeV retains a smaller fraction of events, leading to enhanced statistical fluctuations.

The results of the statistical tests, summarized in the **Table 9**, reveal statistically significant differences between the reduced distributions. The Kolmogorov–Smirnov test yields $D_{05,14} = 0.42$ with $p_{05,14}{}^{D} = 0.0002$ and $D_{05,21} = 0.44$ with $p_{05,21}{}^{D} = 0.0001$, indicating significant shape differences relative to tune 05, with a maximum bin-to-bin deviation of up to 44%. While the ANOVA test shows no significant differences in the mean values ($p_{a,b}{}^{F} > 0.05$ for all $a \neq b$), the Kruskal–Wallis test indicates significant differences in the medians of the distributions for tune pairs 05–14 and 05–21, with $p_{05,14}{}^{H} = 0.0008$ and $p_{05,21}{}^{H} = 0.0003$, respectively.

Table 9. Results of statistical tests for reduced deposited photon energy distributions in the forward detector for *pp* collisions at $E_{CM} = 7.9$ TeV

Tunes	05, 14	05, 21	14, 21
D	0.4200	0.4400	0.1200
p^D	0.0002	0.0001	0.8693
F	0.0062	0.0086	0.0002
p^F	0.9374	0.9262	0.9885
H	11.1790	12.9994	0.1654
p^H	0.0008	0.0003	0.6842

In summary, significant differences between deposited photon energy distributions in the forward detector are observed in the low-energy regions. The very small *P*-values indicate robust sensitivity to the choice of generator tuning. Since such simulations are essential for the design and interpretation of forward-physics experiments, these results underline the importance of an appropriate tuning choice. To further assess the energy dependence of these effects, the analysis is repeated for *pp* collisions at $E_{CM} = 13.6$ TeV.

Distributions of deposited photon energies in pp collisions at $E_{CM} = 13.6$ TeV

Deposited photon energy distributions in the forward detector are examined for *pp* collisions at $E_{CM} = 13.6$ TeV. In the corresponding central detector analysis at this energy, statistically significant differences were observed and attributed to the high-energy part of the photon spectrum. It is therefore of interest to determine whether a similar behaviour is present in the forward detector.

The normalized deposited energy distributions are shown in **Figure 11**, Panel A. Qualitatively, the distributions obtained with tune 05 differ from those generated with the other tuning choices in the lowest-energy bins. This behaviour is quantified by the relative differences shown in **Figure 11**, Panel B, where the largest deviations are observed between tune 05 and the other tunes, while the differences between tunes 14 and 21 remain

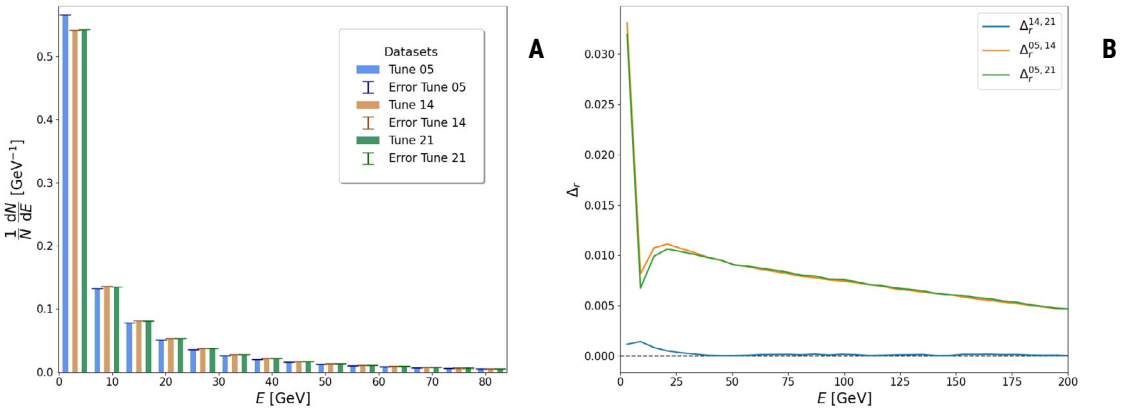

Figure 11. Panel A. Normalized histograms of deposited photon energy distributions in the simulated forward detector for *pp* collisions at E_{CM} = 13.6 TeV. **Panel B.** Relative differences between deposited photon energy distributions in the simulated forward detector for *pp* collisions at E_{CM} = 13.6 TeV.

small across the full energy range. In addition, the relative differences satisfy $\Delta_{r,i}^{05,14} \approx \Delta_{r,i}^{05,21}$ for all bins, suggesting similar statistical behaviour for these tune pairs.

The results of statistical tests, summarized in **Table 10**, confirm this observation. The KS statistics yield identical values, $D_{05,14} = D_{05,21} = 0.1$, matching those obtained at E_{CM} = 7.9 TeV. This indicates that tune 05 produces systematically different distributions in the forward region compared to the other tunes, while the relative shapes of the distributions are largely insensitive to the collision energy. All corresponding *P*-values exceed the significance threshold, demonstrating that the observed differences are not statistically significant.

Table 10. Results of statistical tests for deposited photon energy distributions in the forward detector for *pp* collisions at E_{CM} = 13.6 TeV

Tunes	05, 14	05, 21	14, 21
D	0.1000	0.1000	0.0200
p^D	0.9667	0.9667	1.0000
$F/\times 10^{-2}$	1.3840	1.5552	0.0005
p^F	0.9066	0.9010	0.9942
H	0.5441	0.5646	0.0190
p^H	0.4607	0.4524	0.8903

Overall, these results indicate that, unlike in the central detector, increasing the collision energy to E_{CM} = 13.6 TeV does not lead to statistically significant changes in the deposited photon energy distributions in the forward detector.

Finally, the low-energy region of the deposited photon energy spectrum in the forward detector is examined for *pp* collisions at E_{CM} = 13.6 TeV. The analysis is restricted to $E_{dep} \leq 6$ GeV, and the resulting normalized distributions are shown in the **Figure 12**, Panel A, with the lowest-energy bin omitted for clarity. A pronounced excess of events generated with tune 05 relative to the other tunes is observed in the first displayed bins.

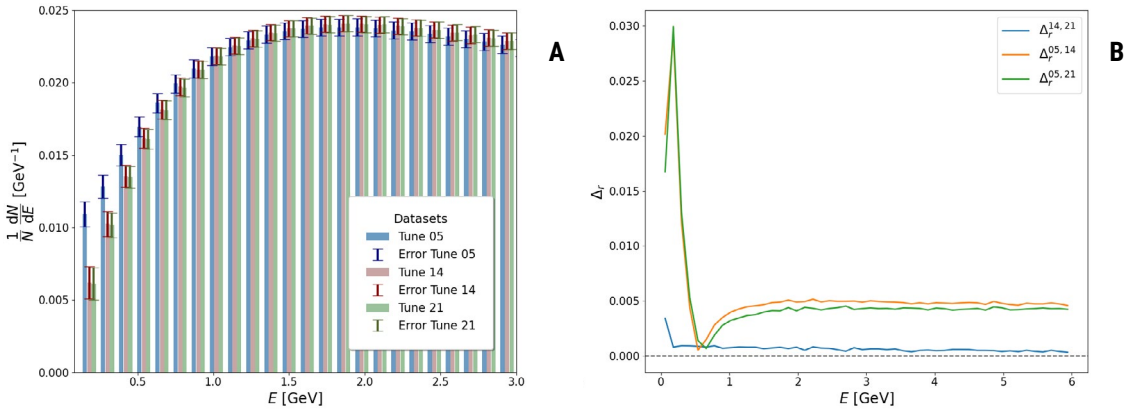

Figure 12. Panel A. Normalized histograms of reduced deposited photon energy distributions in the simulated forward detector for *pp* collisions at E_{CM} = 13.6 TeV. **Panel B.** Relative differences between reduced deposited photon energy distributions in the simulated forward detector for *pp* collisions at E_{CM} = 13.6 TeV.

The corresponding relative differences are presented in **Figure 12**, Panel B. Differences between tunes 14 and 21 remain small across the reduced energy range, while the largest deviations are observed between tune 05 and the other tunes. These differences peak in the lowest-energy bins and decrease with increasing deposited energy, eventually saturating at $\Delta_r \sim 0.005$. As in the full-spectrum analysis, the relation $\Delta_{r,i}^{05,14} \approx \Delta_{r,i}^{05,21}$ holds for all bins.

Statistical tests applied to the reduced distributions, summarized in **Table 11**, confirm these observations. The Kolmogorov–Smirnov test yields maximum shape differences of up to 42% for the tune pair 05-14 and 44% for 05–21, with corresponding *P*-values below 0.05, indicating statistically significant differences. While the ANOVA test shows no significant differences in the mean values, the Kruskal–Wallis test indicates significant differences in the medians for both tune pairs, with $p_{05,14}{}^{H}, p_{05,21}{}^{H} < 0.05$.

Table 11. Results of statistical tests for reduced deposited photon energy distributions in the forward detector for *pp* collisions at E_{CM} = 13.6 TeV

Tunes	05, 14	05, 21	14, 21
D	0.4200	0.4400	0.0400
p^D	0.0002	0.0001	0.9999
$F/\times 10^{-3}$	3.3358	4.3600	0.0073
p^F	0.9541	0.9475	0.9932
H	11.7390	12.1200	0.0017
p^H	0.0006	0.0005	0.9670

Overall, the forward-detector analyses consistently show that distributions generated with tune 05 exhibit systematically different behaviour compared to the other tuning choices, whereas tunes 14 and 21 yield mutually consistent results. This constitutes a key finding of the present study.

Discussion

In this work, distributions obtained using three different tuning choices of the PYTHIA event generator were systematically compared. In total, 5.985×10^8 high-energy proton-proton collision events were simulated across multiple configurations, yielding photon final states. For each distribution, normalized histograms with statistical uncertainties were constructed, relative differences between distributions were evaluated, and multiple statistical tests were applied to assess their compatibility.

Photon transverse momentum distributions were studied for three generator configurations. As expected, the largest relative differences were observed in the low-p_T region; however, when the full p_T range was considered, no statistically significant differences were found. While some relative differences between the distributions obtained with central tunes are present (for example, in tunes 14 and 21), we find that these are not statistically significant but rather arise from bin-to-bin fluctuations in the histograms and do not reflect genuine differences in the underlying distributions. An analysis of the photons originating from neutral pion decays at two different collision energies demonstrated that the magnitude and pattern of these differences depend on the center-of-mass energy of the *pp* collisions.

Detector-level effects were investigated by simulating the response of an electromagnetic calorimeter based on an inorganic scintillator. For the central detector, deposited photon energy distributions were studied at $E_{CM} = 7.9$ TeV and $E_{CM} = 13.6$ TeV, including inactive detector regions to model realistic experimental conditions. While no significant differences were observed at lower energies, statistically significant deviations emerged at $E_{CM} = 13.6$ TeV, originating from the high-energy part of the photon spectrum. Statistical tests showed differences in distribution shapes and medians, but not in mean values. It was further estimated that approximately 1.5×10^7 effective collision events per tune are required for a central detector to resolve such differences, corresponding to roughly 10–15 days of continuous data taking at LHC operating conditions.

A complementary analysis was performed for a realistic forward detector configuration. In this case, statistically significant differences between tuning choices were observed primarily in the reduced, low-energy part of the deposited photon energy spectrum. Distributions generated with tune 05 consistently exhibited behaviour distinct from those obtained with tunes 14 and 21, while the latter two showed mutual compatibility.

Table 12. Summary of statistical comparisons of deposited photon energy distributions in different detector configurations

	Central detector		Forward detector	
E_{CM}	Full spectrum	Reduced spectrum	Full spectrum	Reduced spectrum
7.9 TeV	Statistical tests indicate that the distributions are not significantly different. Local shape differences of up to 12% are observed.	Statistical tests indicate that the distributions are not significantly different. Local shape differences of up to 4% are observed.	Statistical tests indicate that the distributions are not significantly different. Local shape differences of up to 4% are observed.	Statistical tests indicate that the distributions are significantly different. Local shape differences of up to 44% are observed.
13.6 TeV	Statistical tests indicate that the distributions are significantly different. Local shape differences of up to 40% are observed.	Statistical tests indicate that the distributions are not significantly different. Local shape differences of up to 8% are observed.	Statistical tests indicate that the distributions are not significantly different. Local shape differences of up to 10% are observed.	Statistical tests indicate that the distributions are significantly different. Local shape differences of up to 44% are observed.

The largest observed differences in the forward detector reached up to 44% in distribution shape.

In summary, this study identifies the detector configurations and kinematic regions in which tuning-dependent effects become statistically significant and characterizes their nature. The strongest sensitivity to tuning choices is found in deposited photon energy distributions measured in the forward detector. A summary of the statistical test results for different detector configurations is provided in **Table 12**. Analyses of this type constitute an essential step in the design and optimization of future high-energy physics experiments.

Finally, the results highlight a broader implication: no single generator tuning can be regarded as a perfect description of reality, owing to the intrinsic stochastic nature of Monte Carlo simulations. Instead, each tuning provides complementary insight into different aspects of QCD processes. The iterative interplay between the detector development, experimental measurements, and event generator tuning remains crucial for improving both simulations and our understanding of hadronic collisions.

Provenance: This manuscript is based on the master's thesis by Marko Husar, deposited in the Dabar repository (https://urn.nsk.hr/urn:nbn:hr:217:925054).

Peer review: Externally reviewed.

Received: 3 March 2026 / **Accepted:** 12 May 2026 / **Published online:** 2 June 2026.

Data availability: The source codes used to simulate energy deposition in the central and forward detectors are available in the Dabar repository (see Appendices A and B): https://urn.nsk.hr/urn:nbn:hr:217:925054. Additional data are available upon request.

Funding: This study received no funding.

Authorship declaration: MH conducted the literature review, developed the simulation codes, and wrote the manuscript. NP conceived the original research topic and supervised the student during the preparation of the manuscript.

Disclosure of interest: The authors completed the ICMJE Disclosure of Interest Form (available upon request from the corresponding author) and disclose no relevant interests.

ORCID

Marko Husar https://orcid.org/0009-0001-8583-2716

Nikola Poljak https://orcid.org/0000-0002-4512-9620

References

1. Thomson M. Modern Particle Physics. Cambridge (UK): Cambridge University Press; 2013.
2. Peskin ME, Schroeder DV. An Introduction to Quantum Field Theory. Bota Raton (FL): CRC Press; 2018.
3. Yagi K, Hatsuda T, Miake Y. From Big Bang to Little Bang. Cambridgke (UK): Cambridge University Press; 2005.

4. Bierlich C, Chakraborty S, Desai N, Gellersen L, Helenius I, Ilten P, Lönnblad L, Mrenna S, Prestel S, Preuss CT, Sjöstrand T. A comprehensive guide to the physics and usage of PYTHIA 8.3. SciPost Physics Codebases. 2022 Nov 10:008.
5. Skands P, Carrazza S, Rojo J. Tuning PYTHIA 8.1: the Monash 2013 tune. Eur Phys J C. 2014 August;74(8):3024. https://doi.org/10.1140/epjc/s10052-014-3024-y
6. Corke R, Sjöstrand T. Interleaved parton showers and tuning prospects. J High Energy Phys. 2011 March;2011(3):1–52. https://doi.org/10.1007/JHEP03(2011)032
7. Buckley A, Butterworth J, Gieseke S, Grellscheid D, Höche S, Hoeth H, et al. General-purpose event generators for LHC physics. Phys Rep. 2011 July 1;504(5):145–233. https://doi.org/10.1016/j.physrep.2011.03.005
8. Buckley A. ATLAS Pythia 8 tunes to 7 TeV data. ATL-PHYS-PROC-2014-273. In: Proceedings of the Sixth International Workshop on Multiple Partonic Interactions at the Large Hadron Collider; 2014 Nov 3–17; Krakow, Poland.
9. Stephens MA. EDF statistics for goodness of fit and some comparisons. J Am Stat Assoc. 1974 September 1;69(347):730–7. https://doi.org/10.1080/01621459.1974.10480196
10. Berger VW, Zhou Y. Kolmogorov–Smirnov test: Overview. In: Balakrishnan N, Colton T, Everitt B, Piegorsch W, Ruggeri F, Teugels JL, editors. Wiley statsref: Statistics reference online. Hoboken (NJ): Wiley StatsRef: Statistics Reference Online; 2014.
11. Kim TK. Understanding one-way ANOVA using conceptual figures. Korean J Anesthesiol. 2017 January 26;70(1):22. https://doi.org/10.4097/kjae.2017.70.1.22
12. Kruskal WH, Wallis WA. Use of ranks in one-criterion variance analysis. J Am Stat Assoc. 1952 December 1;47(260):583–621. https://doi.org/10.1080/01621459.1952.10483441
13. Adams J, Aggarwal MM, Ahammed Z, Amonett J, Anderson BD, Arkhipkin D, et al. Forward neutral pion production in p+ p and d+ Au collisions at s NN= 200 GeV. Phys Rev Lett. 2006 October 13;97(15):152302. https://doi.org/10.1103/PhysRevLett.97.152302
14. Navas S, Amsler C, Gutsche T, Hernández-Rey JJ, Lourenço C, Masoni A, et al. Review of particle physics. Phys Rev D. 2024;110(3):030001, https://doi.org/10.1103/PhysRevD.110.030001
15. Leo WR. Techniques for nuclear and particle physics experiments. Nucl Instrum Methods Phys Res. 1988;834:290.
16. Viehhauser G, Weidberg T. Detectors in particle physics: a modern introduction. Bota Raton (FL): CRC Press; 2024 Mar 6.
17. Moszynski M, Czarnacki W, Syntfeld-Kazuch A, Nassalski A, Szczesniak T, Swiderski L, et al. A comparative study of undoped NaI scintillators with different purity. In: Sellin P, editor. 2008 IEEE Nuclear Science Symposium Conference Record; 2008 Oct 19–25; Dresden, Germany. New York (NY): Institute of Electrical and Electroncis Engineers; 2008. p. 1138–1144.
18. Van Sciver WJ, Bogart L. Fundamental studies of scintillation phenomena in NaI. IRE Trans Nucl Sci. 1958 December 31;5(3):90–2. https://doi.org/10.1109/TNS2.1958.4315632